Electronic supplementary information:
Nano- and micro-patterning biotemplated magnetic CoPt arrays

J. M. Galloway,*[ab] S. M. Bird,[c] J. E. Talbot,[d] P. M. Shepley,[a], Ruth C. Bradley,[e] O. El-Zubir,[cf] D. A. Allwood,[e] G. J. Leggett,[c] J. J. Miles,[d] S. S. Staniland[c] and K. Critchley[a]

a. School of Physics and Astronomy, University of Leeds, Woodhouse Lane, Leeds, LS2 9JT, UK.
b. School of Chemistry, Cantock's Close, University of Bristol, Bristol, BS8 1TS, U.K.
c. Department of Chemistry, Dainton Building, Brook Hill, University of Sheffield, Sheffield, S3 7HF, UK.
d. School of Computer Science, University of Manchester, Kilburn Building, Oxford Road, Manchester, M13 9PL, UK.
e. Department of Materials Science and Engineering, Sir Robert Hadfield Building, Maplin Street, University of Sheffield, Sheffield, S1 3JD, UK.
f. Chemical Nanosciecnce Laboratories, School of Chemistry, Bedson Building, University of Newcastle, Newcastle Upon Tyne, NE1 7RU, UK.

*e-mail johanna.galloway@bristol.ac.uk, tel: +00 44 (0) 117 66 1806621

Contents

Experimental methods.

Gold film preparation

Slides were cleaned by sonication for 10 minutes each in; 1% Decon 90, 3-5 rinses of MilliQ water, then isopropanol. Then they were dried with N_2, immersed in dichloromethane for 10 minutes, dried with N_2, immersed in piranha solution (30% H_2O_2, 70% H_2SO_4) for 10 minutes, rinsed 3-5 times with MilliQ water, dried with N_2 and mounted into an Edwards Auto 360 thermal evaporator. Thin-films (100 nm) of gold were evaporated onto 5 nm chromium onto the cleaned glass slides. Gold films were sectioned into ≈1 cm^2 pieces and cleaned with isopropanol, dried with N_2 before treating with UV/ozone (20 minutes, UVOCS) to remove surface contamination, and soaking in ethanol (40 minutes) to reduce the surface back to metallic Au.

Nano-patterning using interference lithography (IL)

An anti-biofouling SAMs were formed on clean gold surfaces by immersion in a solution of alkanethiol (1 mM 11-mercaptoundecyl tetra(ethylene)glycol (PEG) in ethanol) for 24 hours. The surfaces were removed from the SAM forming solution, rinsed in ethanol and dried under N_2. Interference lithography was used to create nano-patterns by exposing the SAM surface to a Coherent Innova 300C FreD frequency doubled argon ion laser beam (λ≈244 nm, maximum power 100 mW) in a Lloyd's mirror arrangement, as described in Tizazu *et al*.[1] The laser beam was expanded to illuminate area of ≈1 cm^2, and was directed towards the surface at a fixed angle of 2θ to the mirror. The laser was positioned so that half of the beam interacted with the sample surface, and the other half reflected off the mirror onto the sample. Interference between the reflected and direct portions of the beam creates an exposure pattern on the SAM surface. The SAMs were exposed for 7-14 minutes to achieve a dose of 20-40 J cm^{-2}, resulting in spatially defined nanoscale photo-oxidation of the SAM on the gold surface.

Stamp master preparation

Patterned stamp masters were formed by UV-photolithography of silicon substrates coated with an epoxy negative tone photoresist (SU8 2002, Microchem. Corp and Chestech, UK). All processing was performed in a class 100 cleanroom. Silicon wafers were sectioned into ≈1 cm^2 pieces before cleaning via sonication for 2 minutes in each: acetone; MilliQ water, isopropanol; then MilliQ. Substrates were dried with a N_2 stream and dehydrated on a hotplate (5 minutes, 150°C). Wafer sections were immersed in piranha solution (30% H_2O_2, 70% H_2SO_4 (v/v)) for 10 minutes before thorough rinsing in MilliQ water and drying with N_2. SU8 photoresist was pipetted onto the cleaned silicon, and the surfaces spun at 2000 rpm for 100 seconds (Suss MicroTec Lithography Delta 6 RC BM AK-200.417 controlled by a Suss MicroTec Delta +10 control unit) and cured on a hotplate (2 minutes, 95°C) to form an average resit thickness of 1.6 μm. The resit build up at the edges of the silicon (the edge bead) was then removed by abrasion. The SU8 was patterned using soft-UV light (365 nm) through a pattern definition mask in contact mode, using a Karl Suss MJB-3 UV mask aligner. The lamp power of the mask aligner was optimised so that the exposure time provided an optimal dose of 21 mJ cm^{-2} to the photoresist. After exposure, the substrates were baked on a hotplate (2 minutes, 95°C), and then gradually cooled to room temperature. The exposed substrates were then developed in an EC11 solution (Microchem) for 1 minute, rinsed in isopropanol and dried under N_2. The patterned masters were then hard baked on a hotplate (10 minutes, 150°C). Cooled masters were rinsed in isopropanol,

dried under N_2, then silanised by evaporating a few drops of a fluorinated silane (1H, 1H, 2H, 2H perfluorooctyltriethoxysilane) onto the micro-patterned surface to create a hydrophobic coating.

Micro-contact printing (μCP)

Patterned masters on silicon were cleaned with propanol and dried with N_2. Poly dimethyl siloxane (PDMS, Sylguard 184 base with w/w 10 % curing agent) was thoroughly mixed, poured over the master, and bubbles removed by degassing under vacuum. The PDMS elastomer was cured overnight (16 hours) at 60°C before the stamps were cut out and soaked in ethanol overnight (16 hours). Stamps were dried with N_2 and inked with an anti-biofouling SAM forming alkanethiol (5 mM 11-mercaptoundecyl tetra(ethylene)glycol (PEG) in ethanol) for 4 minutes. Excess alkanethiol solution was removed via pipette and the stamp thoroughly dried under N_2 prior to micro-contact printing (μCP) onto clean gold surfaces. The stamp was conformally contacted onto the clean gold surface for 4 minutes and then removed before functionalising with the biotemplating cysteine tagged peptide.

Peptide functionalisation of surface

A clean gold surface (unpatterned), a micro-contact printed surface (μCP,) or an interference lithographically patterned surface (IL) was immersed in a solution of 20 μg mL^{-1} of the cys_CoPt biotemplating peptide (C-GSG-KTHEIHSPLLHK, Genscript, > 95% purity) in phosphate buffered saline (PBS from Invitrogen: 10 mM sodium phosphate, 2.68 mM KCl, 140 mM NaCl, pH 7.4). After 1 hour, the substrates were rinsed in water and placed into a water jacketed glass reaction vessel. The sulfur in the cysteine at the *N*-terminus of the peptide has a strong affinity for gold surface binding. This backfilling with the biotemplating peptide creates areas of the surface that resist (PEG SAM) or promote (cys_CoPt) biotemplated mineralisation.

Biotemplated mineralisation

Solutions of cobalt sulfate (Co^{2+}, 30 mM $CoSO_4{\cdot}7H_2O$, 126.5 mg in 15 mL) and sodium tetrachloroplatinate (Pt^{2+}, 10 mM Na_2PtCl_4, 57.4 mg in 15 mL) salts were prepared in deoxygenated MilliQ water (vacuum degassed for >1 hour and sparged with N_2 gas for >1 hour). The reducing agent (sodium borohydride, 25 mM, $NaBH_4$, 28.5 mg in 30 mL) was also prepared in anoxic water just prior to use. 2.5 mL Co^{2+} and 2.5 mL Pt^{2+} were added to the peptide patterned gold substrate and incubated for 5 minutes at 18°C. Cooling was maintained using recirculated water. For the bulk peptide control, 100 μL of a 1 mg mL^{-1} peptide solution (10 μg mL^{-1} in the 10 mL reaction) in PBS was added in place of the peptide patterned substrate. N_2 was flowed through the solutions for the duration of the mineralisation. 5.0 mL of $NaBH_4$ was injected into the reaction vessel. The pink-yellow salt solution is reduced to black metallic particles, both in the bulk solution and onto the peptide immobilised on the gold surface. Biotemplated surfaces were removed from the excess reactants and products after ≈45 minutes, and rinsed 3-5 times in anoxic water and dried with N_2.

Electron microscopy

A Hitachi SU8230 cold field emission (CFE) scanning electron microscope (SEM) was used to image samples at 2-15 keV via the in lens SE(U) detector. Energy dispersive X-ray (EDX) spectra were recorded using an Oxford Instruments AZtecEnergy EDX system on the SEM at 15 keV. A Phillips CM200(FEG)TEM (transmission electron microscope) was used to image bulk precipitated samples dried onto carbon coated copper grids at 200 keV, using the digital micrograph software. EDX spectra

were recorded using an Oxford Instruments INCA EDX system and Gatan Imaging Filter. ImageJ[2] was used to record the average width of the nano- and micro-patterns (20 measurements perpendicular to the line pattern), error quoted is the standard deviation of these measurements. ImageJ was also used to record the length and width of ≈400 particles for each sample. The average diameter for each particle was binned into ≈20 bins and fitted with Gaussian distributions in Origin:

$$y = y_0 + \frac{A}{w\sqrt{\pi/2}} e^{\frac{-2(x-x_c)^2}{w^2}}$$

Where y_0 is the offset, x_c is the centre, w is the width and A the amplitude of the symmetric peak. The aspect ratio was also binned into ≈20 bins, and fitted with asymmetric distributions using the Extreme fitting tool in Origin:

$$y = y_0 + Ae^{(-e^{(-z)}-z+1)}$$
$$z = (x - x_c)/w$$

Where y_0 is the offset, x_c is the centre, w is the width and A the amplitude of the asymmetric peak. The average aspect ratio (error one standard deviation) was also calculated.

X-ray diffraction (XRD)

A Brucker-AXS D8 series2 diffractometer set to a Bragg Brentano Parafocussing Geometry was used to record diffraction spectra. X-rays were generated using a Cu-Kα source at 40 kV at room temperature. Monochromated X-rays were passed through a 2 mm exit slit and an automatic divergence slit of 0.2°. Diffraction intensity was collected at angles of 2θ between 2° and 80° on a Braun position sensitive detector (0.02° and 6.0 seconds per step). These diffraction data were processed using AXS Commander and EVA software.

Vibrating sample magnetometry (VSM)

The biomineralised sample was mounted and centered to maximise the signal from the magnetic surface to the detector. Hysteresis loops were measured with the field perpendicular and parallel to the surface with a Microsense Model 10 vector VSM, using an applied field of -5 to 5 kOe at a sweep rate of 500 Oe s^{-1} at 295 K.

Magneto-optical Kerr effect (MOKE)

Measurements were taken in the polar and longitudinal geometries. A HeNe laser (λ=633 nm) was directed through a polariser onto the sample at an incident angle of 0° (polar) or ~30° (longitudinal) from the surface normal. A magnetic field of up to 6 kOe can be applied out-of-plane (polar) or at any angle in the plane (longitudinal). The polarisation of the light rotates as it is reflected from the ferromagnetic material. The change in the Kerr signal during a field sweep is measured by passing the light through a second polariser and measuring the change in intensity incident on a photodiode. Polar MOKE is sensitive only to the out-of-plane component of magnetisation, whereas longitudinal MOKE is sensitive to the in-plane magnetisation along the direction defined by the applied in-plane field.

Magnetic force microscopy (MFM)

Force microscopy plots were recorded using MFM tips (Cr/Co coated MESP probes, Brucker). These tips were magnetised parallel to the long axis of the tip (i.e. perpendicular to the surface) before mounting onto the piezohead of a Multimode Nanoscope III. To obtain maps of both topography and

magnetic interactions, the Nanoscope software was used to position the detection at the center of the resonant frequency of the cantilever and at a phase shift of 0°. The surface topography was recorded in tapping mode at the resonant frequency of the cantilever. This height trace was then followed in non-contact mode at a lift height above the height of the particles (25-50 nm) to minimise impacts, and thus record magnetic interactions as positive (repulsion) and negative (attraction) phase shifts in the resonance of the cantilever. By selecting an appropriate lift height, phase information can be attributed to the magnetised tip interacting with the magnetic particles on the surface rather than artefacts introduced by the tip contacting the surface. These MFM data were processed (flattened and scale limits set) using WSxM[3] and Nanoscope Analysis v1.50, and 3D plots generated in 'R' using the rgl package. 3D rendering script available at: https://github.com/jonbramble/MFMPlot.

Supplementary Figures

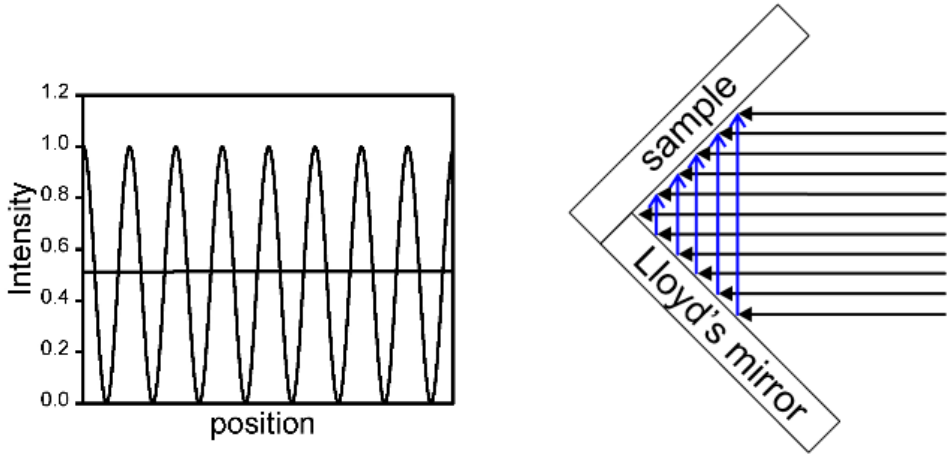

Fig. S1. Diagram to show pattern generation by interference lithography (IL)[1]. On the left is a sketch of a typical intensity profile that is generated by the constructive and destructive interference of the laser. This interference is generated by a Lloyd's mirror arrangement, shown on the right. Areas of constructive interference on the surface remove an adsorbed self-assembled monolayer (SAM), whereas areas of destructive interference leave the SAM intact to create nano-lines on the surface.

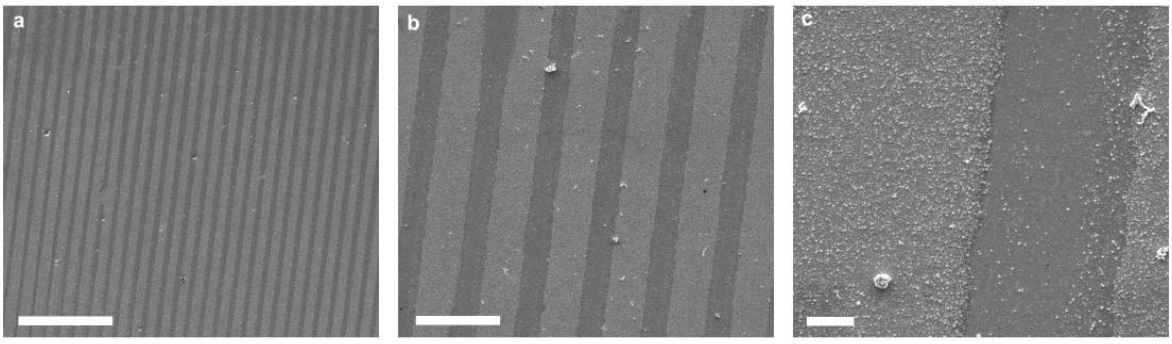

Fig. S2. Scanning electron microscope (SEM) images of biotemplated patterned lines, biomineralised at 18°C at (a) low, (b) medium and (c) high magnifications. Lines of dark contrast are the gold surface that was protected against biomineralisation by the µCP PEG thiol. Lines of light contrast were backfilled with the biotemplating cys_CoPt peptide before metallisation with CoPt, and are covered in a biotemplated layer of MNPs. Scale bars (a) 100 µm, (b) 20 µm, and (c) 2 µm.

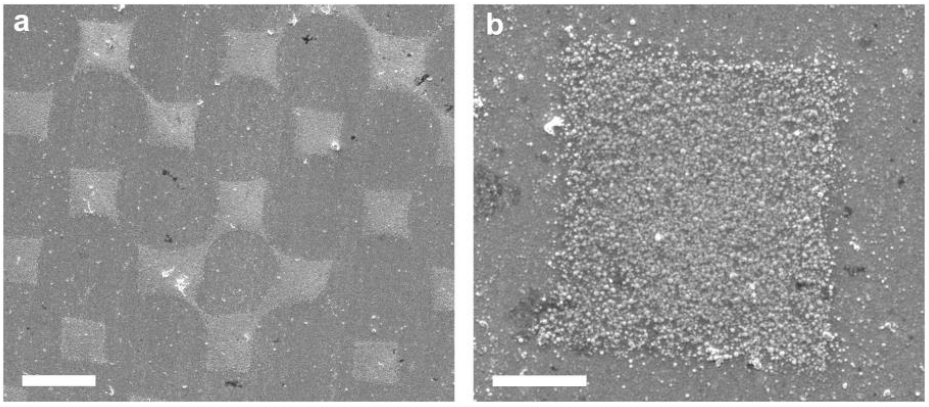

Fig. S3. Scanning electron microscope (SEM) images of biotemplated patterned squares, biomineralised at 18°C at (a) low, and (b) high magnifications. Light contrast squares are peptide biotemplated CoPt MNPs, dark contrast background is protected against metallisation by μCP PEG thiol. Scale bars (a) 10 μm and (b) 2 μm.

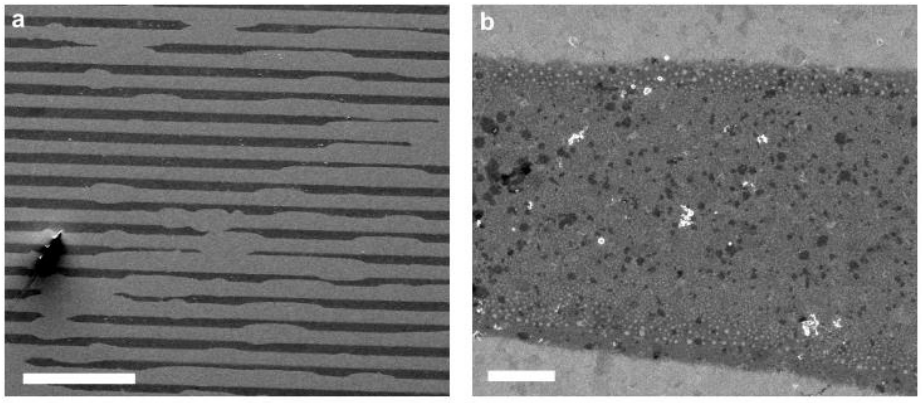

Fig. S4. Scanning electron microscope images (SEM) of biotemplated patterned lines metallised at a higher temperature of ≈35°C. (a) The areas functionalised with the cys_CoPt biotemplating peptide (dark contrast) are unable to template MNPs. At higher magnification (b) the biotemplating areas can be seen to be coated in a thin discontinuous layer of black and white speckling. It is likely that the higher temperatures in the lab in summer significantly increased the rate of the metallisation reaction. The higher temperatures may also have reduced the solubility of CoPt MNP precursors and/or inhibited the ability of the CoPt biotemplating peptide immobilised on the surface to bind to the forming particles. For any or all of these reasons, the biotemplating peptide is not able to control the mineralisation of MNPs onto surfaces at 35˚C, but instead forms this thin, discontinuous film. Scale bars (a) 100 μm and (b) 1 μm.

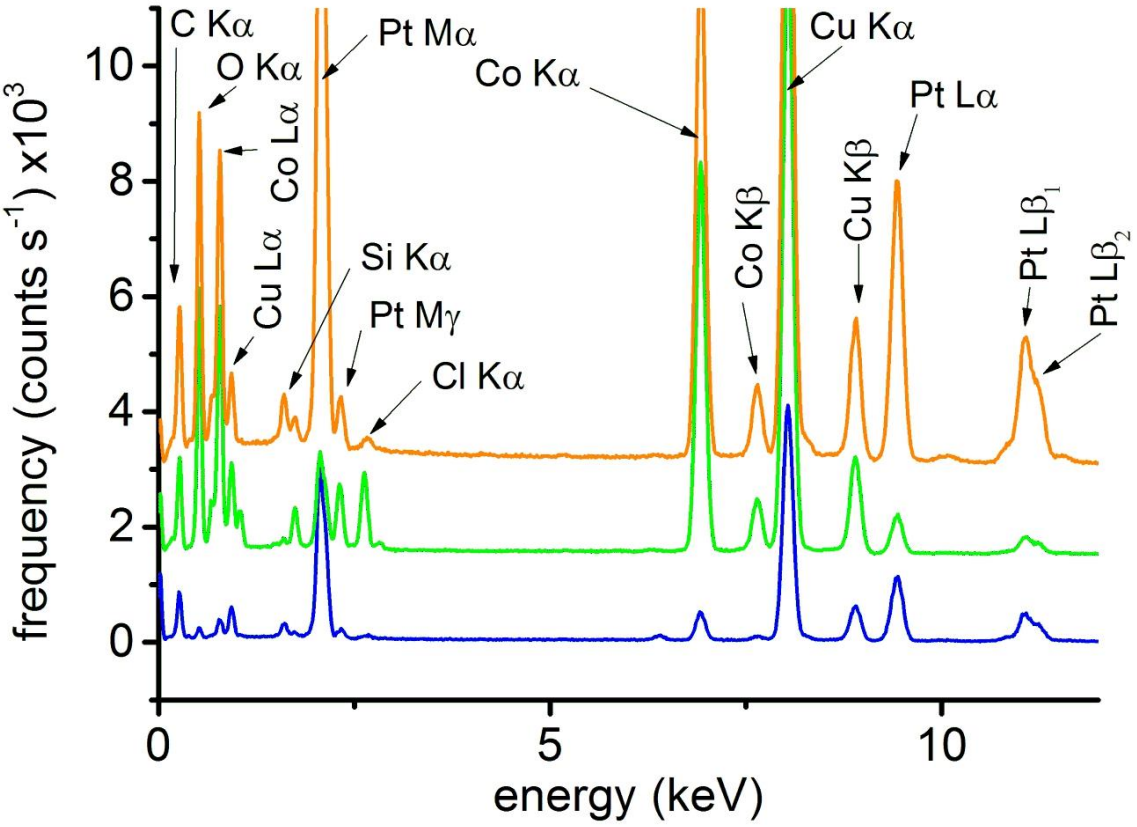

Fig. S5. Energy dispersive X-ray (EDX) spectra from the powder control samples recorded in the TEM. All samples show peaks that pertain to the formvar carbon coated copper grids (Cu, C, O, Si), and chlorine is probably from the buffer the peptide was stored in (PBS). The non-peptide bulk templated particles (**blue**) also show peaks for Co and Pt, with quantification showing atomic percentage ratio of 25:75. Quantification of the non-cysteine tagged peptide bulk templated particles (**green**) Co:Pt is 88:12, and the cys_CoPt bulk templated particles (**orange**) is 59:41. The stoichiometry of Co:Pt in the metallisation solution was 75:25, and the ideal ratio for $L1_0$ CoPt is 50:50. Despite the large excess of Co in the mineralisation solution, the bulk precipitated particles are dominated by Pt, so much of the Co must remain unreacted in the solution. It is likely that much of the Co detected in the peptide templated samples may be bound by the organic peptide matrix. As there was no detection of Co reflections in the SAED (see Fig. S7 below), this indicates that the peptide is able to bind cobalt well, and may form an amorphous or poorly crystalline cobalt phase that can be seen to surround the MNPs.

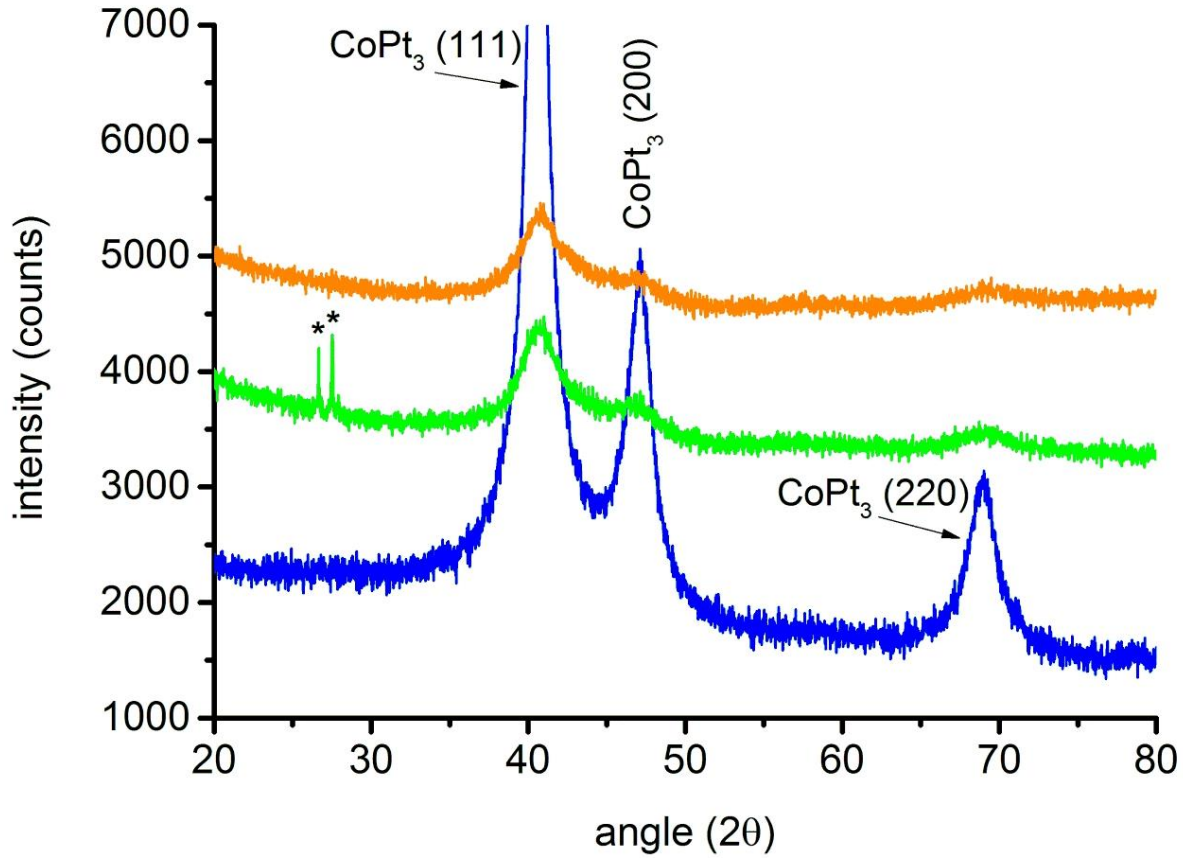

Fig. S6. X-ray diffraction (XRD) data for the powder controls. Bulk precipitated (**blue**), bulk peptide biotemplated (**green**) and bulk cysteine tagged peptide biotemplated (**orange**) powders show strong peaks for $CoPt_3$ rather than the CoPt $L1_0$ structures. There are also two peaks, labelled with asterisks (*****) that are likely to be due to carbon in this biotemplated sample. Scans are vertically offset for clarity, and details of peak assignments are shown in Table S1.

Table S1. Peak positions, corresponding d-spacing and peak assignments for surfaces (see Fig. 4f) and powder controls (see Fig. S6). The measured peak positions are converted to *d*-spacings using Bragg's Law ($n\lambda = 2dsin\theta$), where *n* is 1, λ is the wavelength of the incident X-rays (1.5406 Å), *d* is the spacing between the planes in Å, and ϑ is the angle between the incident ray and the scattering planes. The material and *hkl* lattice spacings are assigned based on the closest match between the measured spectra and standard spectra in the JCPDS data base.

sample	2θ (°)	$d_{measured}$ (Å)	$d_{reference}$ (Å)	compound name	h	k	l	formula	JCPDS No.
bulk	40.54	2.22	2.22	cobalt platinum	1	1	1	$CoPt_3$	00-029-0499
	47.09	1.93	1.93	cobalt platinum	2	0	0	$CoPt_3$	00-029-0499
	68.97	1.36	1.36	cobalt platinum	2	2	0	$CoPt_3$	00-029-0499
peptide bulk	26.61	3.35	-	carbon	-	-	-	C	Wang *et al.* (2012)[4]
	27.54	3.24	-	carbon	-	-	-	C	
	40.73	2.21	2.22	cobalt platinum	1	1	1	$CoPt_3$	00-029-0499
	47.09	1.93	1.93	cobalt platinum	2	0	0	$CoPt_3$	00-029-0499
	69.24	1.36	1.36	cobalt platinum	2	2	0	$CoPt_3$	00-029-0499
cysteine tagged peptide	40.83	2.21	2.22	cobalt platinum	1	1	1	$CoPt_3$	00-029-0499
	47.27	1.92	1.93	cobalt platinum	2	0	0	$CoPt_3$	00-029-0499
	69.24	1.36	1.36	cobalt platinum	2	2	0	$CoPt_3$	00-029-0499
clean gold surface	38.30	2.35	2.36	gold FCC	1	1	1	Au	00-004-0784
	44.56	2.03	2.04	gold FCC	2	0	0	Au	00-004-0784
	64.78	1.44	1.44	gold FCC	2	2	0	Au	00-004-0784
	77.77	1.23	1.23	gold FCC	3	1	1	Au	00-004-0784
	81.82	1.18	1.18	gold FCC	2	2	2	Au	00-004-0784
cysteine tagged peptide on surface	23.99	3.71	3.68	$L1_0$ cobalt platinum	0	0	1	CoPt	00-029-0498[5]
	29.00	3.08	-	carbon	-	-	-	C	Wang *et al.* (2012)[4]
	29.65	3.01	-	carbon	-	-	-	C	
	38.34	2.35	2.36	gold FCC	1	1	1	Au	00-004-0784
	40.79	2.21	2.17	$L1_0$ cobalt platinum	1	0	1	CoPt	00-029-0498
	44.53	2.03	2.04	gold FCC	2	0	0	Au	00-004-0784
	47.51	1.91	1.90	$L1_0$ cobalt platinum	1	1	0	CoPt	00-029-0498
	64.74	1.44	1.44	gold FCC	2	2	0	Au	00-004-0784
	77.70	1.23	1.23	gold FCC	3	1	1	Au	00-004-0784
	81.82	1.18	1.18	gold FCC	2	2	2	Au	00-004-0784

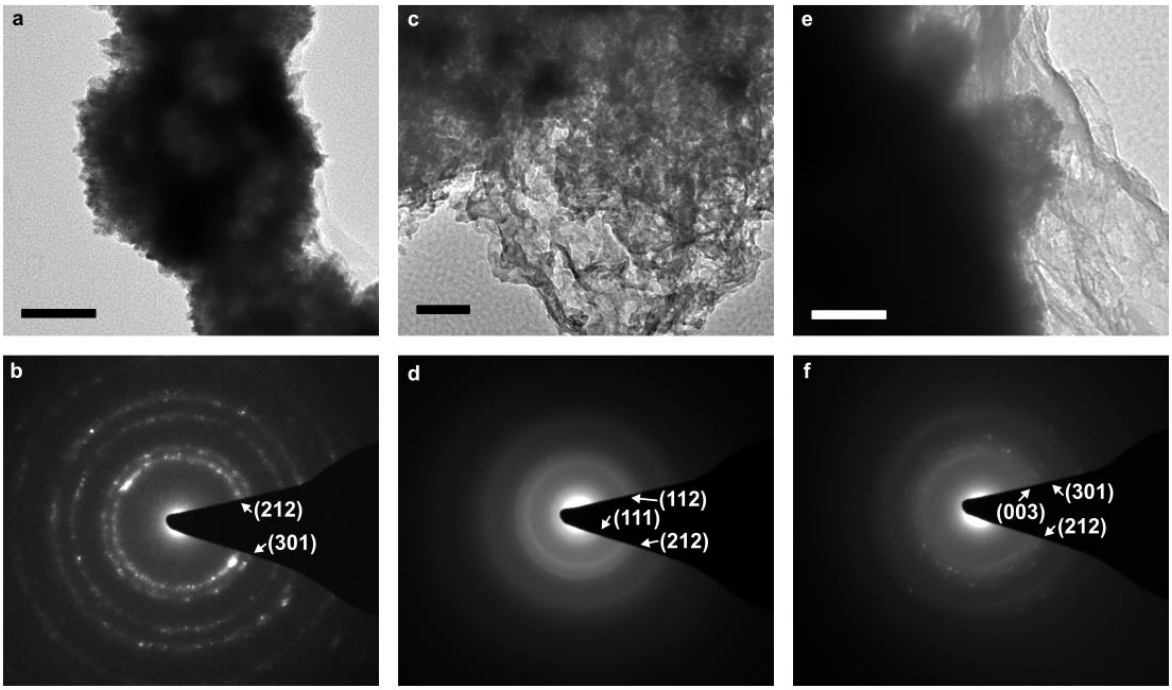

Fig. S7. Transmission electron microscope (TEM) and selected area electron diffraction (SAED) of the controls for the biotemplated surface MNPs. The TEM images (a, c & e) show clusters of multiple particles, which are likely self-assembled due to magnetic interactions between the particles. This made imaging and diffraction on these samples difficult. (a) TEM image of bulk precipitated particles in the absence of any biotemplating peptide (bulk) and (b) SAED pattern showing reflections for A1 CoPt. (c) TEM image of MNPs templated with a non-cysteine tagged version of the CoPt peptide in the bulk solution (peptide), with the particles imbedded in a matrix of material that looks like it is organic. (d) SAED pattern from this sample, showing reflections for $CoPt_3$ (111) and A1 CoPt (112) and (212). (e) TEM image of MNPs templated by the cysteine tagged CoPt templating peptide in the bulk solution (cys_CoPt), again the particles seem to be embedded in a matrix that looks like organic material. (f) SAED diffraction pattern from the cys_CoPt peptide in the bulk solution templated particles, showing $L1_0$ CoPt reflections (003) and A1 reflections (212) and (301). Details of indexing is shown in Table S2. Scale bars 50 nm.

Table S2. Table to show indexing of SAED patterns shown in Fig. S7 above. For each sample, the measured radius (*r*) has been converted to a *d* spacing using ($d = \frac{\lambda l}{r}$), where λ is the wavelength of the electrons (0.025 mm) and *l* is the camera length (170 mm). The material and *hkl* lattice planes have been assigned based on comparison of the measured *d*-spacing to standards from the JCPDS data base, which are also shown.

sample	r (1/nm)	d (Å) measured	d (Å) nearest	sample name	h	k	l	formula	JCPDS No.
bulk	4.18	1.02	1.00	cobalt platinum	2	1	2	CoPt	00-029-0498
	4.87	0.87	0.87	cobalt platinum	3	0	1	CoPt	00-029-0498
	6.87	0.62	-	n/a	-	-	-	-	-
	8.07	0.53	-	n/a	-	-	-	-	-
	10.66	0.40	-	n/a	-	-	-	-	-
peptide	1.90	2.24	2.22	cobalt platinum	1	1	1	$CoPt_3$	00-029-0499
	3.27	1.30	1.32	cobalt platinum	1	1	2	CoPt	00-029-0498
	4.15	1.02	1.00	cobalt platinum	2	1	2	CoPt	00-029-0498
	6.05	0.70		n/a	-	-	-	-	-
cys_CoPt	3.46	1.23	1.23	cobalt platinum	0	0	3	CoPt	00-029-0498
	4.19	1.01	1.00	cobalt platinum	2	1	2	CoPt	00-029-0498
	4.84	0.88	0.87	cobalt platinum	3	0	1	CoPt	00-029-0498
	6.89	0.62		n/a	-	-	-	-	-

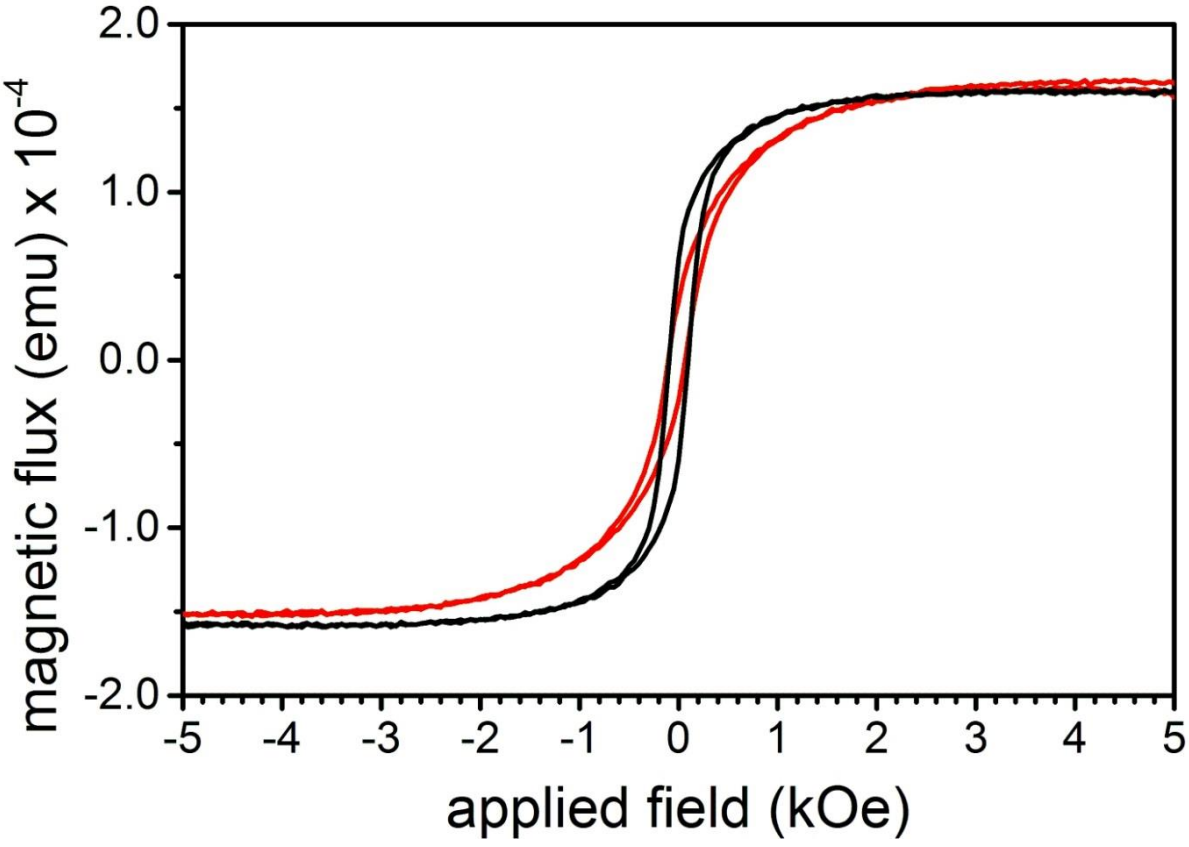

Fig. S8. Vibrating sample magnetometry (VSM) measurements of a biotemplated CoPt surface. Loops were recorded with the field applied perpendicular (**red**) or parallel (**black**) to the sample surface. The lower gradient (loop shear) seen in the perpendicular loop (**red**) may be due to shape anisotropy of the film contributing to demagnetising effects.

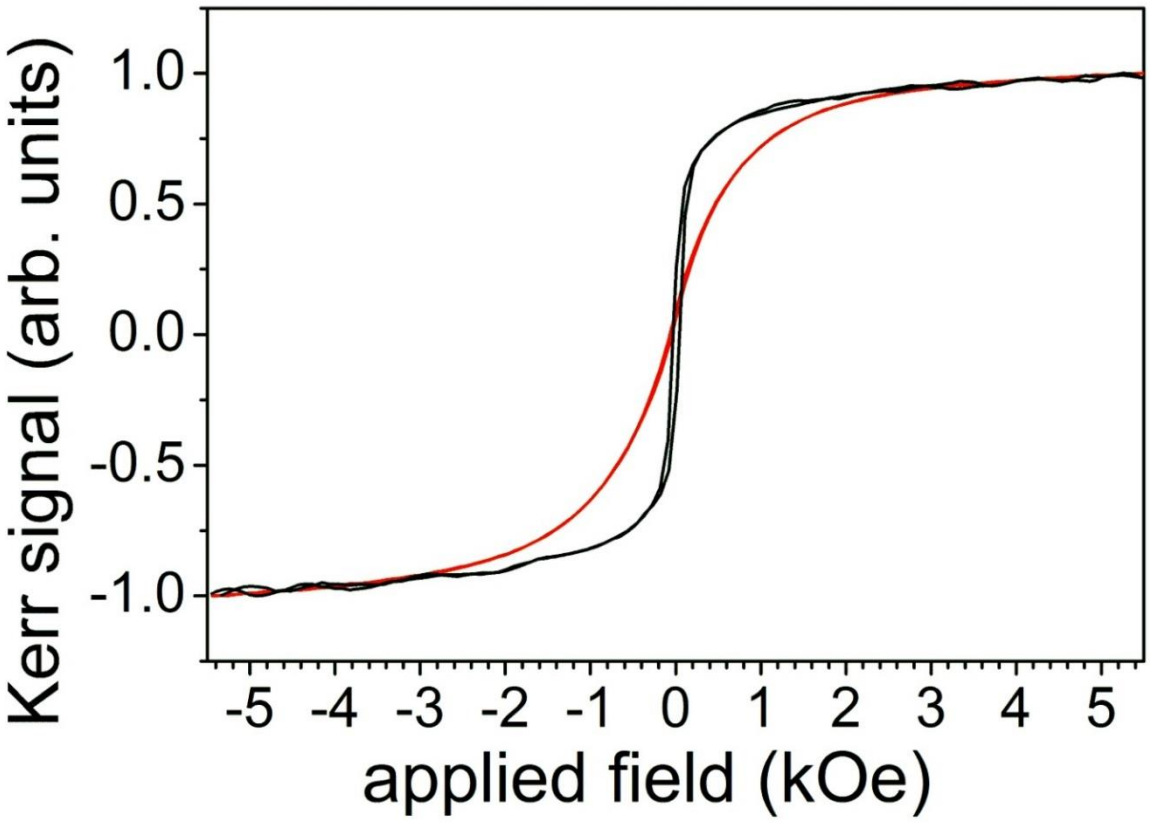

Fig. S9. Magneto-optical Kerr effect (MOKE) measurements of a biotemplated CoPt surface. There is little difference between the width of the hysteresis loops (the coercivity) measured perpendicular (**red**) or parallel (**black**) to the sample surface. The loop shear seen in the perpendicular VSM measurements (Fig. S8) is also observed in these MOKE measurements.

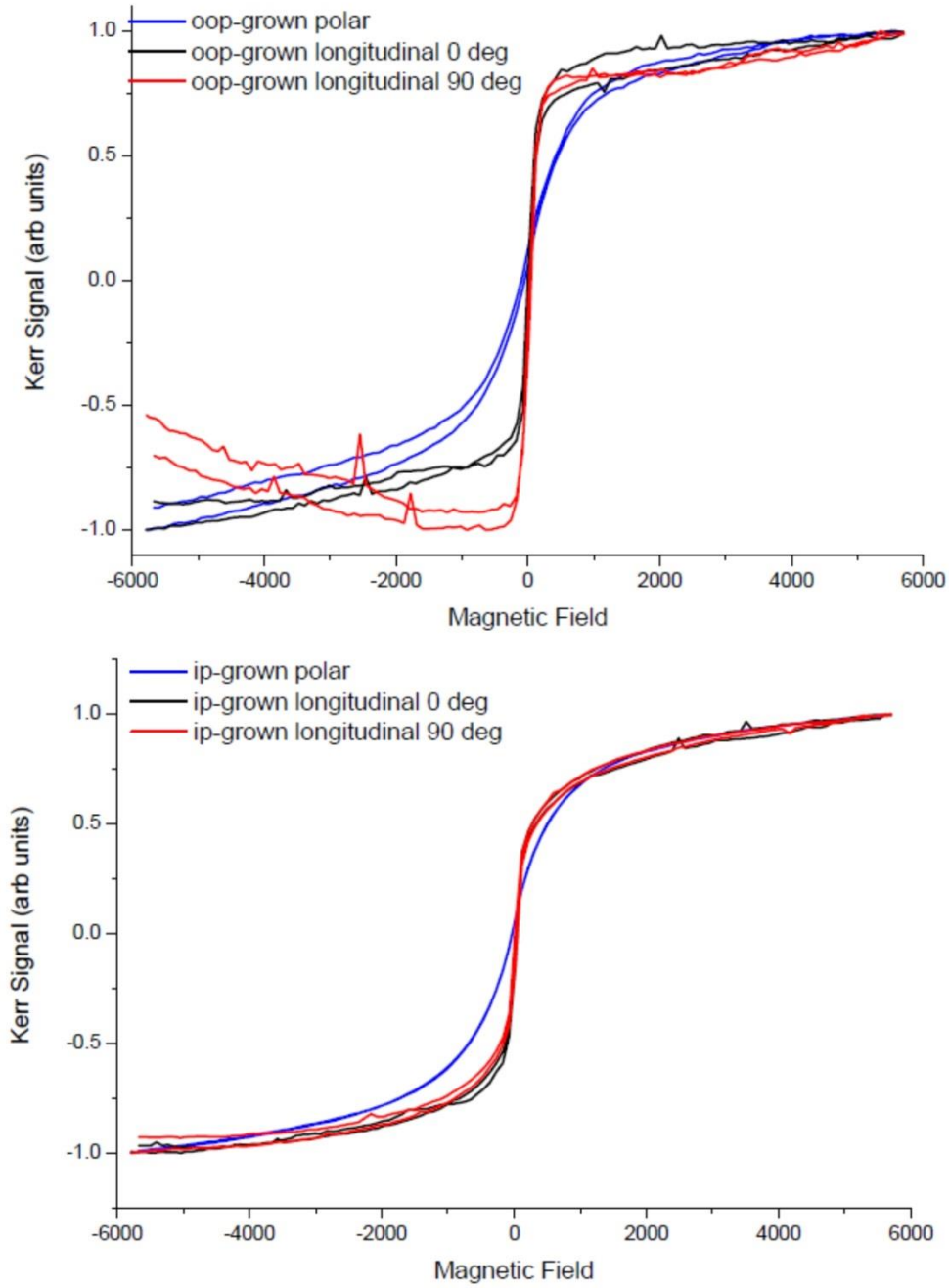

Fig. S10. Hysteresis loops recorded using MOKE on biotemplated surfaces formed (a) perpendicular and (b) parallel to a 0.2 T DC field. The loops show that the samples are ferromagnetic, but have low coercivity. Samples biomineralised with the field applied out-of-plane (oop, (a)) and in-plane (ip, (b)). The hysteresis loops were recorded at 90˚ to the surface (polar) and then parallel to the surface at two different angles (longitudinal 0˚ and 90˚) to measure the magnetic response of the surfaces in the *x*, *y*, and *z* planes. Again, the MNPs have a more rapid switching when the field is applied in-plane for the measurements when compared to it being applied out-of-plane.

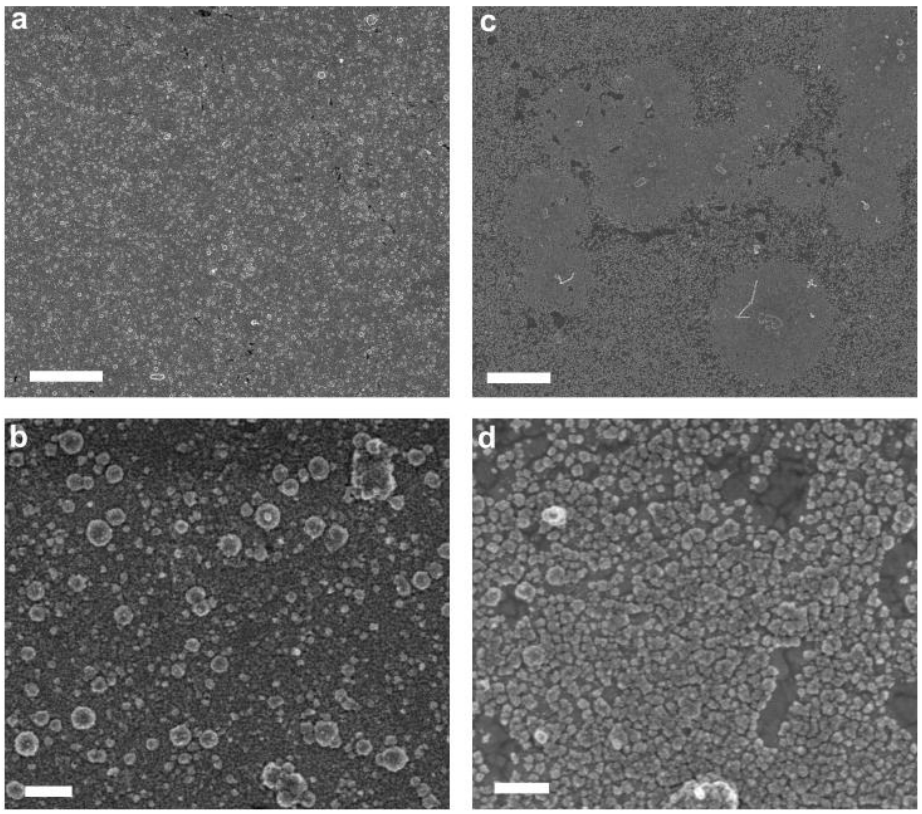

Fig. S11. Scanning electron microscopy (SEM) of unpatterned biotemplated surfaces metallised in the presence of an applied field of 0.2 T. (a & b) Biotemplated CoPt MNPs formed when the field is applied parallel to the surface during mineralisation. (c & d) Biotemplated CoPt formed when the field is applied perpendicular to the surface during mineralisation. Scale bars (a & c) 2 µm and (b & d) 200 nm.

Supplementary discussion of Fig. S11:

Mineralisation in an applied field was unable to align the $L1_0$ *c*-axis. To try and align the particles with the *c*-axis perpendicular to the film, we performed the mineralisation in the presence of an applied magnetic field. A 0.2 T DC field was applied either perpendicular or parallel to unpatterned biotemplating surfaces for the duration of the mineralisation reaction (the stages shown in Fig. 1e-f). MOKE measurements on these surfaces showing no increase in coercivity (Fig. S10). However, Fig. S11 shows that the samples mineralised with the surface parallel to the field look identical to those formed with no applied field (Fig. 2). Those metallised with the field perpendicular to the biotemplating surface are cleaner (i.e. have less adsorbed supra-particles), but the MNPs are more patchily distributed on the surface. We continued this study on those samples mineralised in the absence of an applied field, to ensure a consistent layer of biotemplated MNPs, since discontinuous layers are undesirable for data storage applications.

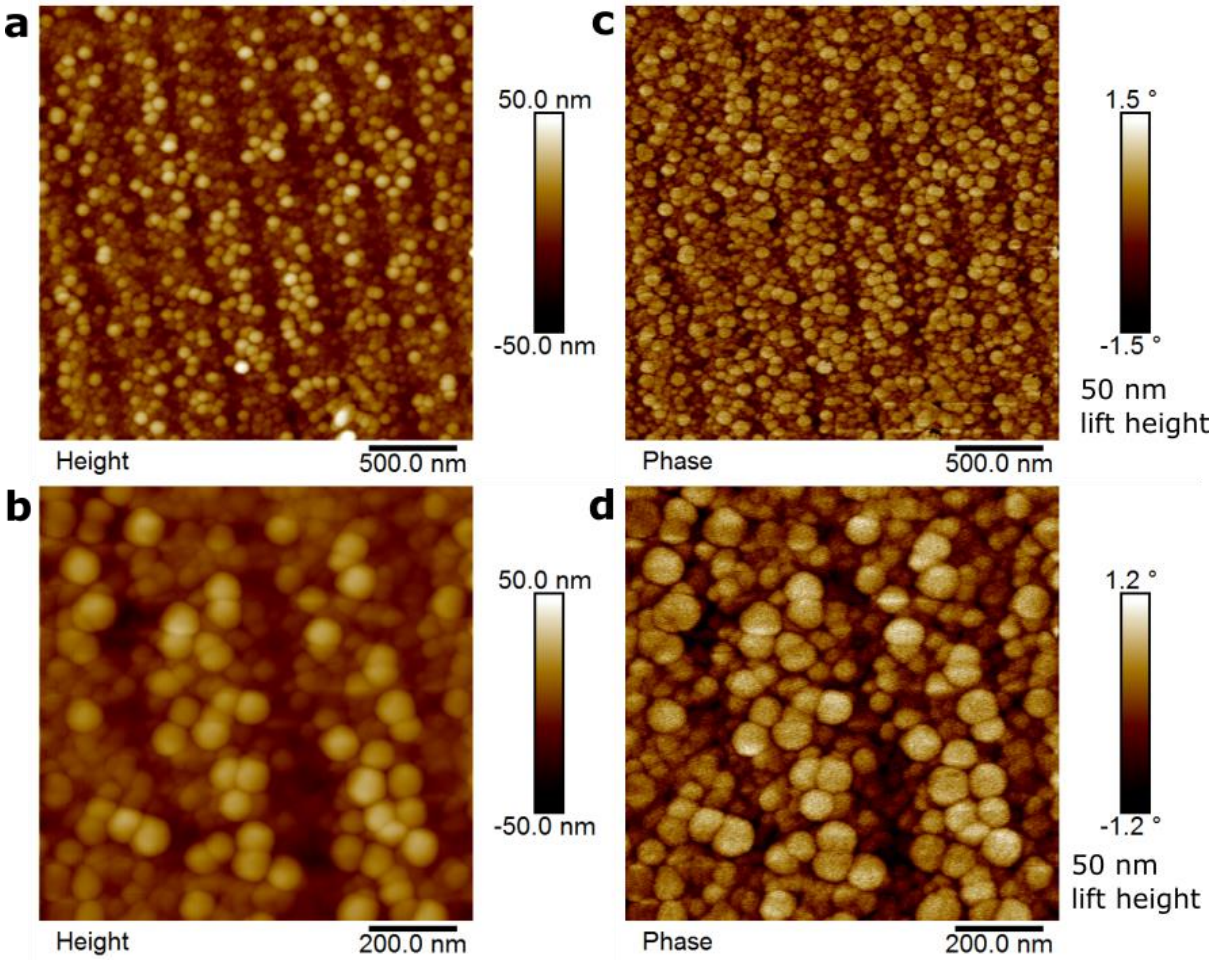

Fig. S12. Separate magnetic force microscopy (MFM) of nano-patterned surfaces. (a & b) Tapping mode height, and (c & d) the respective phase contrast due to magnetic interactions between the magnetised tip and the IL nano-patterned MNPs biotemplated onto the surface. The magnetic nanoparticles show mainly repulsion (light) that extend across multiple MNPs on the surface. These same plots are shown combined in Fig. 5a & b.

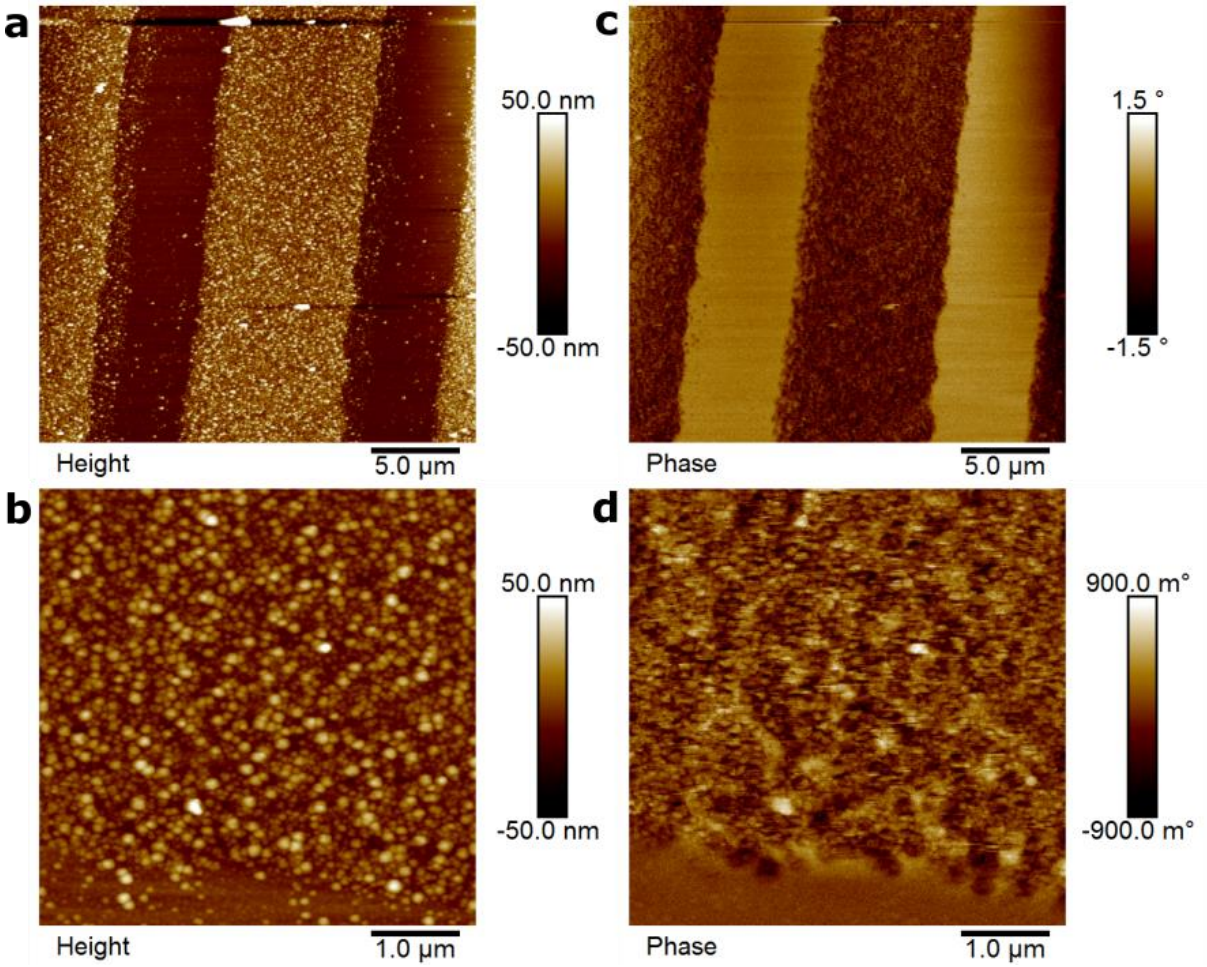

Fig. S13. Separate MFM of micro-patterned surfaces. Separated scans to show the height contrast (a & b) and corresponding phase contrast in non-contact mode (c & d) of the µCP MFM plots also shown in Fig. 5c & d. 25 μm^2 scan area of biotemplated µCP CoPt line patterned surface, a topography recorded in tapping mode and c phase shift recorded at a lift height of 50 nm. There is significant attraction of a few degrees between the magnetised tip and the patterned biotemplated CoPt MNPs. 5 μm^2 scan area (b) topography and (d) phase contrast recorded at a lift height of 50 nm and a 90° angle to image (a). Here, the gold substrate appears as close to zero (i.e. non-magnetic) in the phase shift when compared to the MNPs. The magnetic nanoparticles clearly show zones of attraction (**dark**) and repulsion (light) that extend across multiple MNPs on the surface.

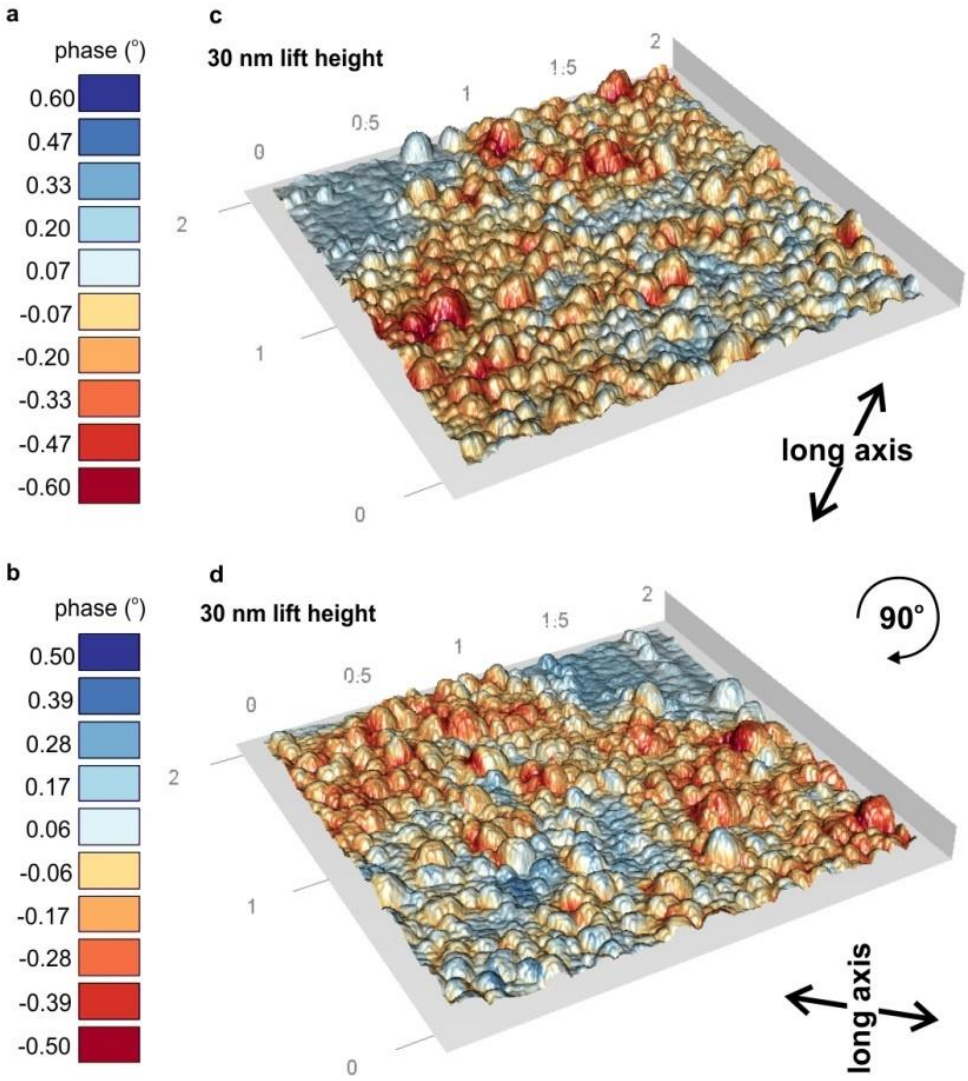

Fig. S14. Combined MFM plots of same area of line micro-patterned biotemplated CoPt MNPs, scanned at a 45° angle to the line pattern. (a & b) colour keys to show phase shift in plots (c & d) respectively A negative phase shift indicates attraction (**red**) between the tip and the surface, and a positive phase shift indicates repulsion (**blue**). (c) 2 μm^2 scan area of biotemplated CoPt surface, topography recorded in tapping mode and phase shift recorded at a lift height of 30 nm. (d) 2 μm^2 scan of the same area recorded at a lift height of 30 nm with the scan direction rotated by 90°. Both plots show similar zones of attraction and repulsion that extend across multiple MNPs on the surface, parallel to the long axis of the line pattern. These are shown as separated height and magnetic plots in Fig. S15.

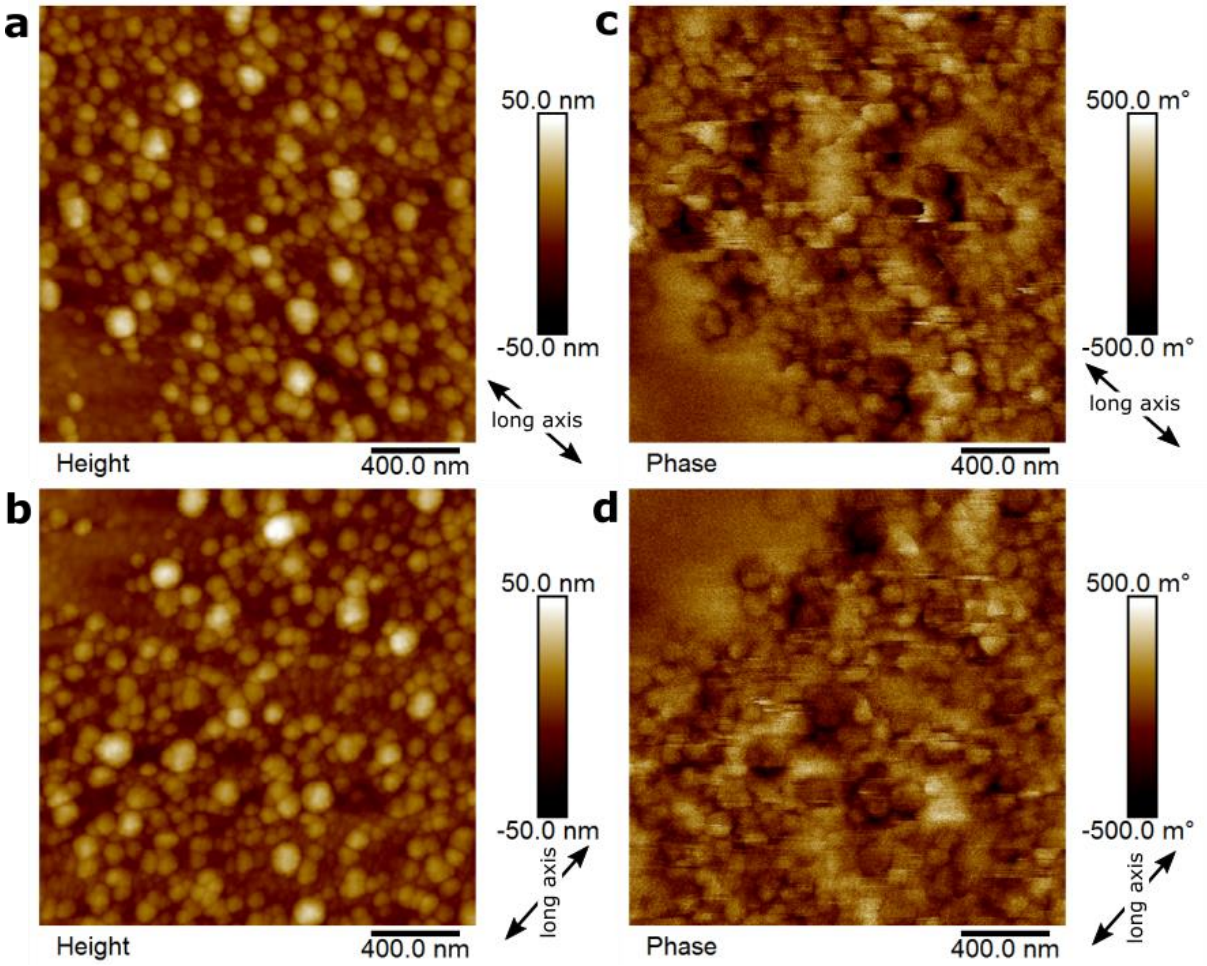

Fig. S15. Separate MFM plots of the same area of line micro-patterned biotemplated CoPt MNPs, scanned at + and - 45° angle to the line pattern, also shown in Fig. S14 as combined plots. (a & b) Height plots recorded in tapping mode at a 90˚C angle to each other, and (c & d) the respective phase contrast recorded at a lift height of 30 nm. Arrows indicate the direction of the long axis of the micro-patterned lines on the surface. The magnetic nanoparticles show zones of attraction (**dark**) and repulsion (light) that extend across multiple MNPs on the surface. Magnetic phase contrast appears to align with the long axis of the pattern, indicating that shape anisotropy of the assembly influences the magnetic alignment of the biotemplate MNPs.

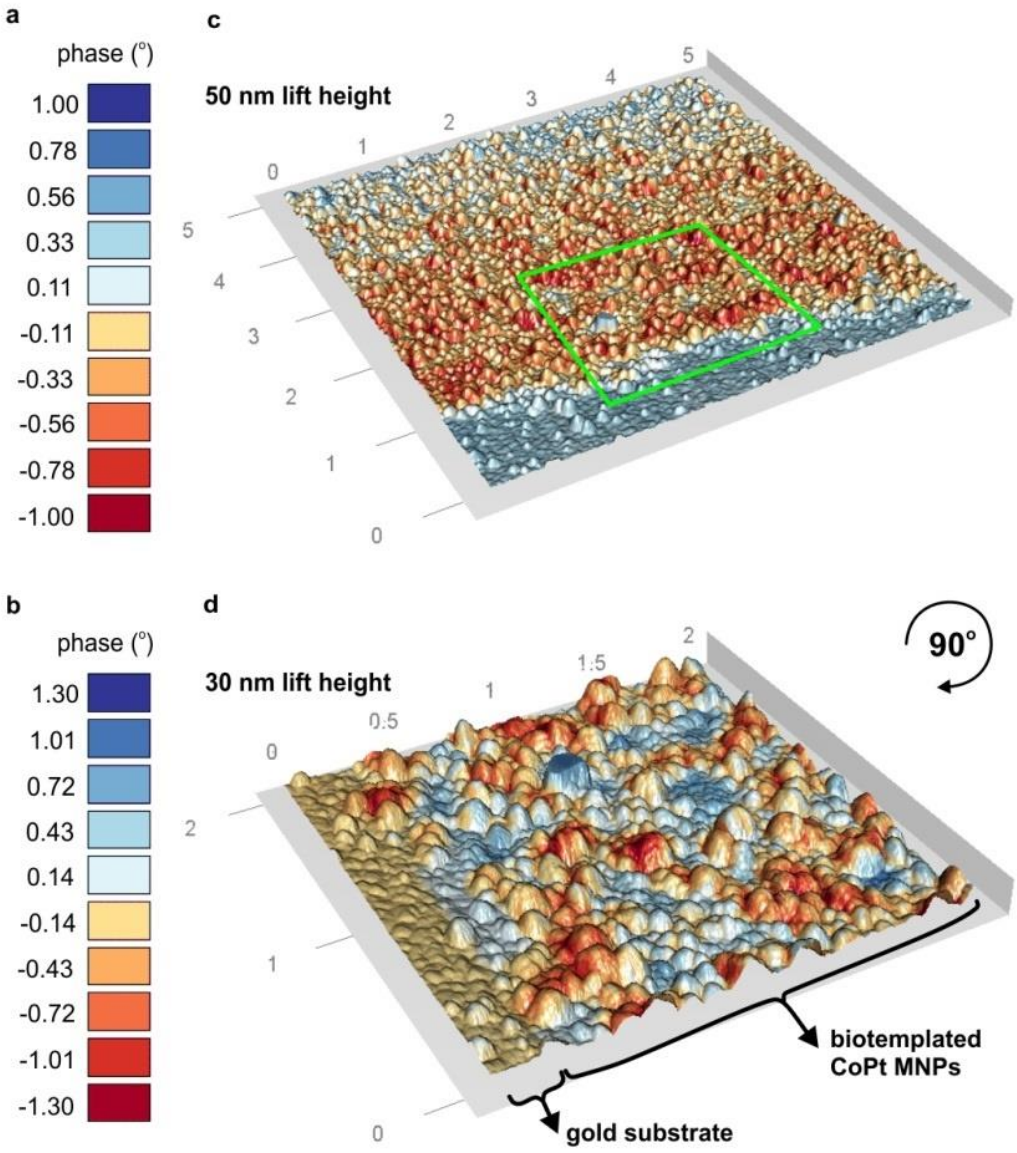

Fig. S16. Combined MFM plots of biotemplated CoPt micro-patterned surface. (a & b) colour keys to show phase shift in plots (c & d) respectively A negative phase shift indicates attraction (**red**) between the tip and the surface, and a positive phase shift indicates repulsion (**blue**). (c) 5 μm^2 scan area of biotemplated CoPt line patterned surface, topography recorded in tapping mode and phase shift recorded at a lift height of 50 nm, green area highlights area scanned for image (d). d, 2 μm^2 scan area recorded at a lift height of 30 nm and a 90° angle to image (c). Again, both plots clearly show zones of attraction and repulsion that extend across multiple MNPs on the surface. Again, these zones appear to run roughly parallel to the long axis of the patterned biotemplated lines, even when the scale of the image and the scan direction is changed. These are shown as separate height and magnetic contrast plots in Fig. S17**.**

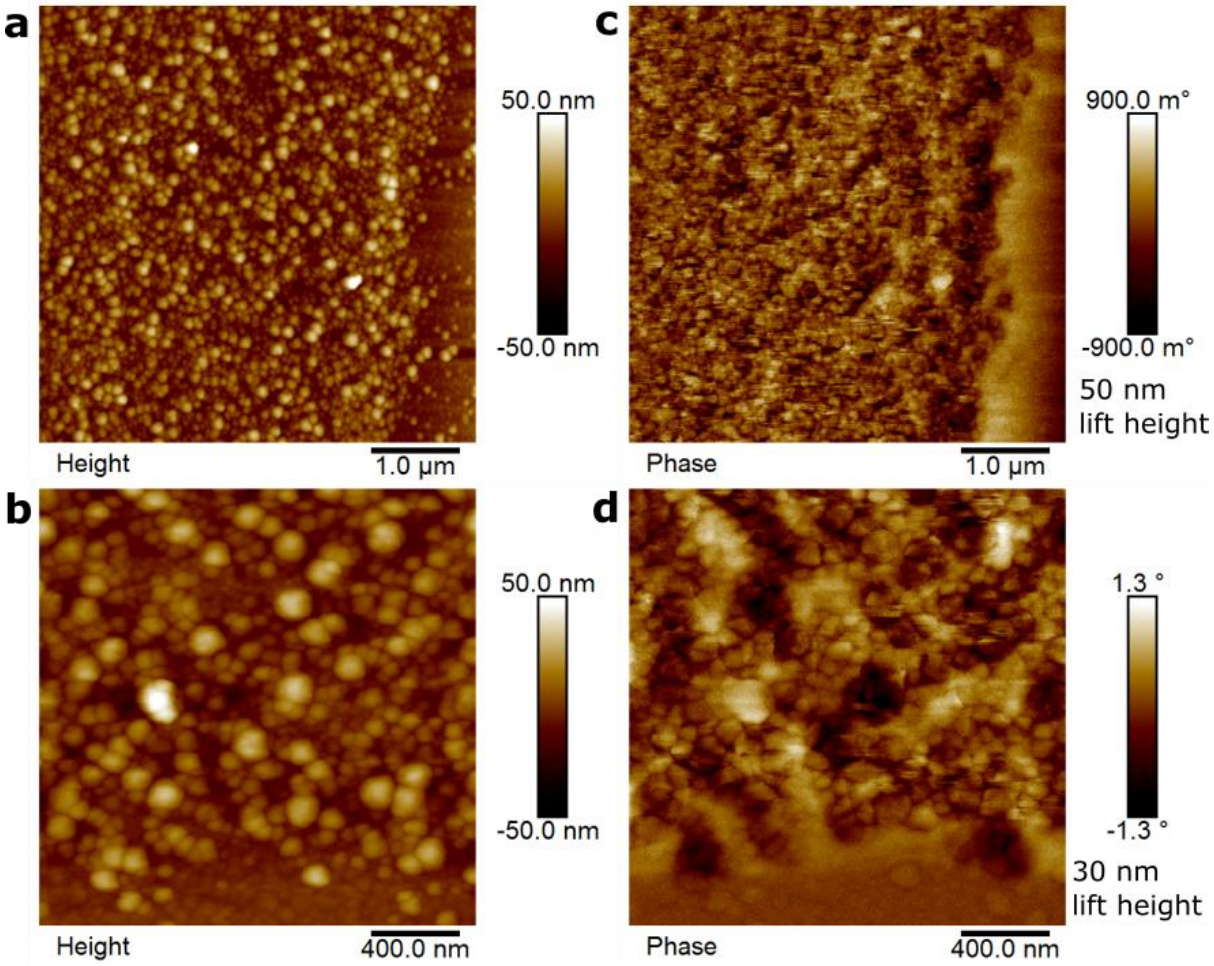

Fig. S17. Separate MFM plots of micro-patterned surfaces. (a & b) Tapping mode height, and (c & d) the respective phase contrast due to magnetic interactions between the magnetised tip and the MNPs biotemplated onto the surface. The magnetic nanoparticles show significant zones of attraction (**dark**) and repulsion (light) that extend across multiple MNPs on the surface. These same plots are shown combined in Fig. S16.

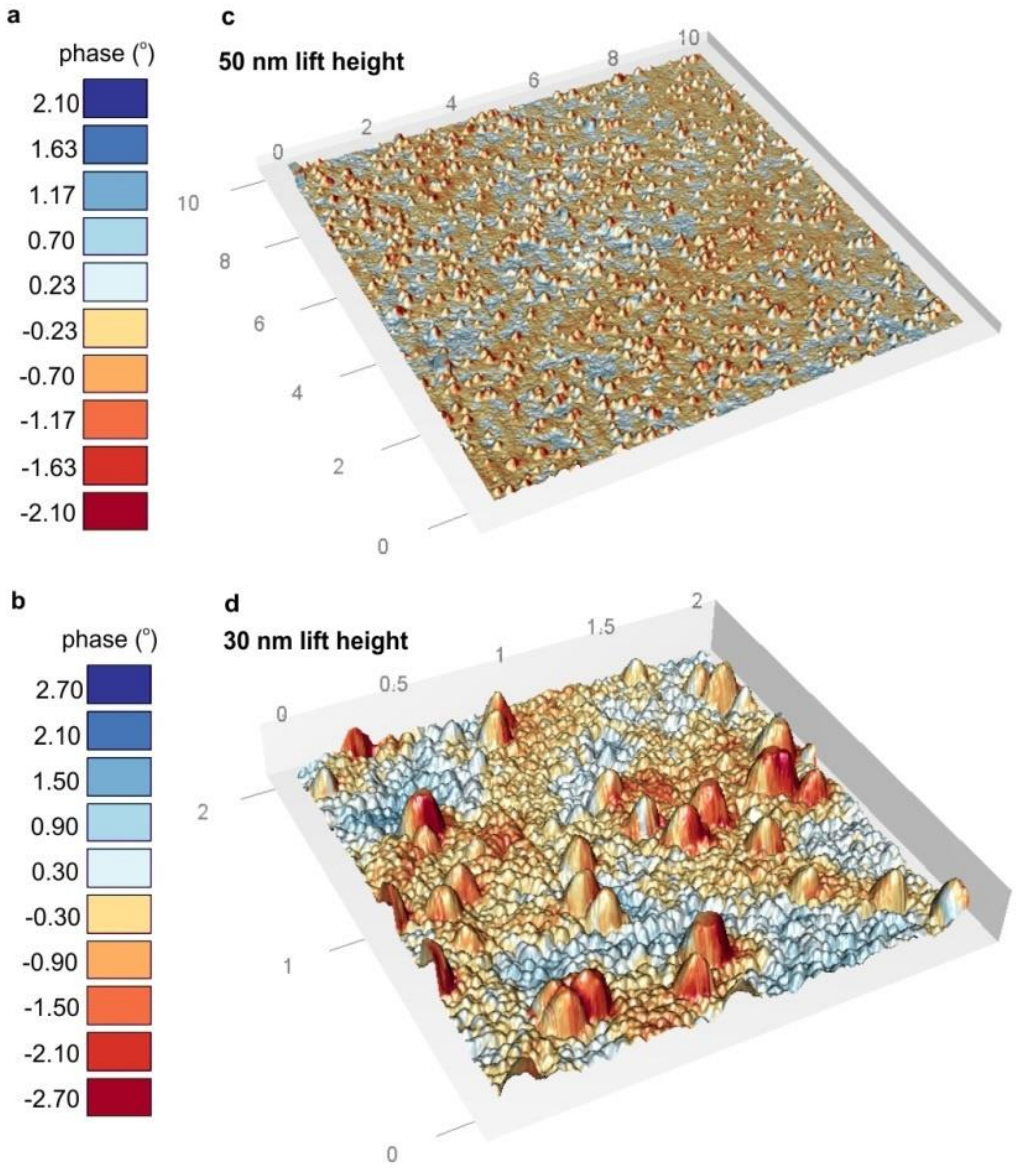

Fig. S18. Combined MFM plots of biotemplated CoPt unpatterned surface. (a & b) colour keys to show phase shift in plots (c & d) respectively A negative phase shift indicates attraction (**red**) between the tip and the surface, and a positive phase shift indicates repulsion (**blue**). (c) 10 μm^2 scan area of biotemplated CoPt surface, topography recorded in tapping mode and phase shift recorded at a lift height of 50 nm. (d) 2 μm^2 scan area recorded at a lift height of 30 nm. Both plots clearly show zones of attraction and repulsion that extend across multiple MNPs on the surface. These appear to wider than those observed on the biotemplated lines pattern. They also do not appear to have any preferred alignment or orientation. These are shown as separate height and magnetic plots in Fig. S19.

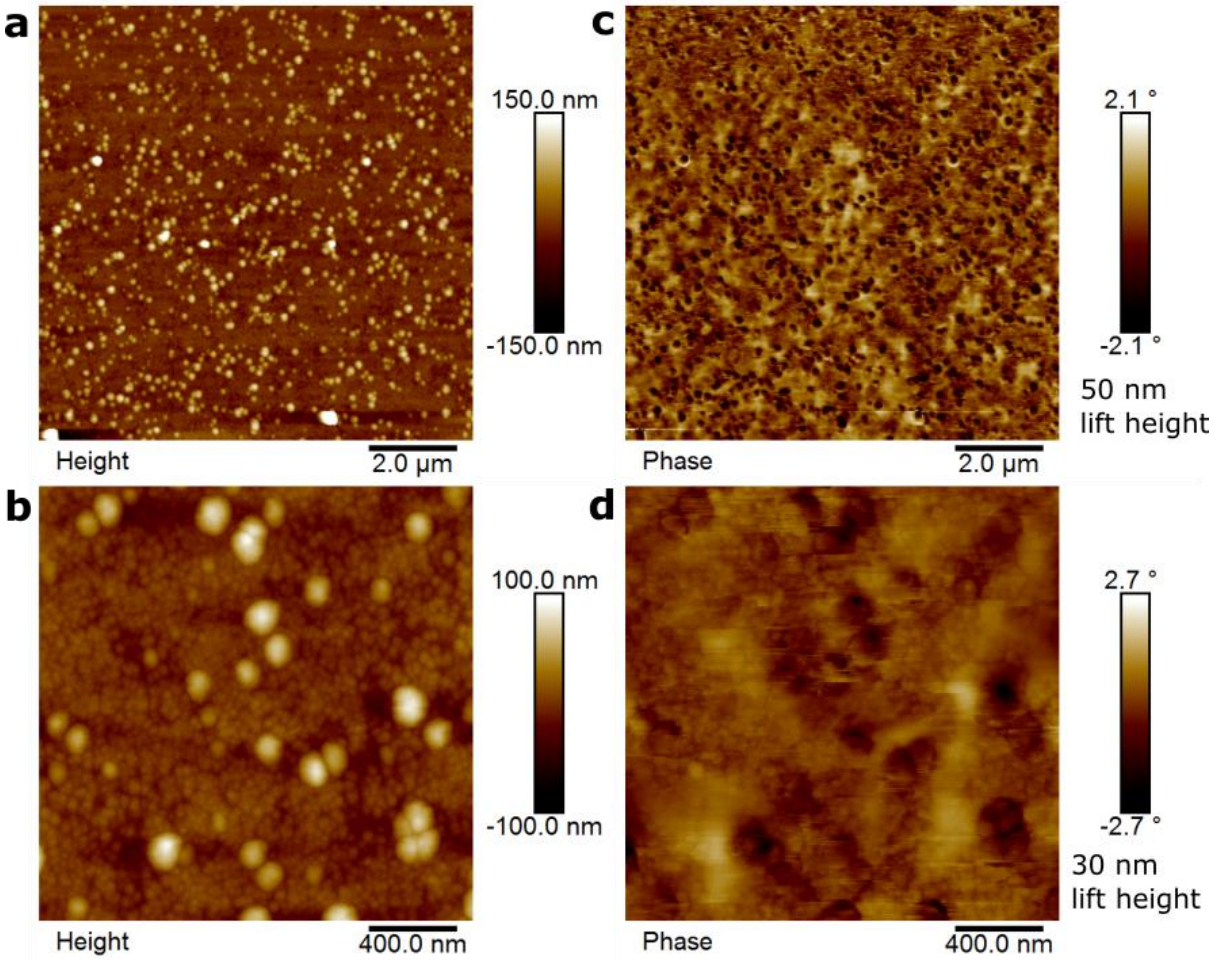

Fig. S19. Separate MFM plots of unpatterned biotemplated CoPt surfaces. (a & b) Tapping mode height, and (c & d) the respective phase contrast due to magnetic interactions between the tip and the unpatterned MNPs biotemplated onto the surface. The magnetic nanoparticles show significant zones of attraction (**dark**) and repulsion (light) that extend across multiple MNPs on the surface. These same plots are shown combined in Fig. S18.

References

1. Tizazu, G. *et al.* Large area nanopatterning of alkylphosphonate self-assembled monolayers on titanium oxide surfaces by interferometric lithography. *Nanoscale* **3,** 2511–2516 (2011).

2. Abramoff, M. D., Magalhaes, P. J. & Ram, S. J. Image processing with Image J. *Biophotonics Int.* **11,** 36–42 (2004).

3. Horcas, I. *et al.* WSXM: a software for scanning probe microscopy and a tool for nanotechnology. *Rev. Sci. Instrum.* **78,** 13705 (2007).

4. Wang, Y., Panzik, J. E., Kiefer, B. & Lee, K. K. M. Crystal structure of graphite under room-temperature compression and decompression. *Sci. Rep.* **2,** Article No. 520 (2012).

5. Wellons, M. S. *et al.* Synthesis of L10 ferromagnetic CoPt nanopowders using a single-source molecular precursor and water-soluble support. *J. Mater. Chem. C* **1,** 5976–5980 (2013).